THE JOURNAL OF PHYSICAL CHEMISTRY C
A JOURNAL OF THE AMERICAN CHEMICAL SOCIETY

pubs.acs.org/JPCC

Article

Pressure-Dependent Magnetic Properties of Quasi-2D $Cr_2Si_2Te_6$ and $Mn_3Si_2Te_6$

Rubyann Olmos, Po-Hao Chang,* Prakash Mishra, Rajendra R. Zope, Tunna Baruah, Yu Liu, Cedomir Petrovic, and Srinivasa R. Singamaneni*

Cite This: *J. Phys. Chem. C* 2023, 127, 10324−10331

Read Online

ACCESS | Metrics & More | Article Recommendations | Supporting Information

ABSTRACT: Recently, pressure has been used to induce structural and magnetic phase transitions in many layered quantum materials whose layers are linked by van der Waals forces. Materials with such weakly held layers allow for relatively easy manipulation of the superexchange mechanism, which can give rise to novel magnetic behavior. Using hydrostatic pressure as a disorderless means to manipulate the interlayer coupling, we applied pressure on two quasi-2D sister compounds, namely, $Cr_2Si_2Te_6$ (CST) and $Mn_3Si_2Te_6$ (MST), up to ∼1 GPa. Magnetic property measurements with the application of pressure revealed that the ferromagnetic transition temperature decreases in CST, while the opposite occurs for the ferrimagnetic MST. In MST, magnetization decreases with the increase in pressure, and such a trend is not clearly observed within the pressure range studied for CST. The overall pressure effect on magnetic characteristics such as exchange couplings and magnetic anisotropy energies is also examined theoretically using density functional theory. Exchange coupling in MST is strongly frustrated, and the first nearest neighbor interaction is the most dominant of the components with the strongest pressure dependence. In CST, the exchange coupling parameters exhibit very little dependence on pressure. This combined experimental and theoretical work has the potential to expand to other relevant quantum materials.

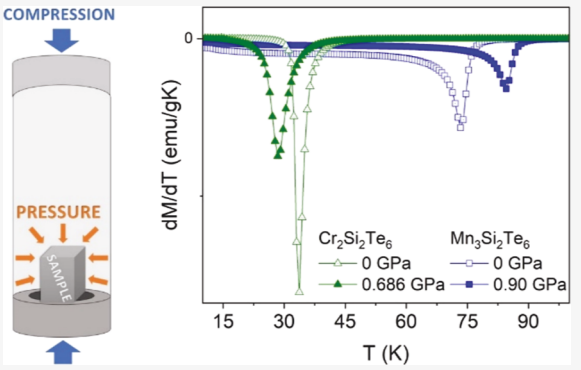

INTRODUCTION

Exploring the magnetic properties of bulk (quasi-2D) crystals serves as a basis for understanding the magnetic phenomena in reduced dimensions (true 2D limit). Profound knowledge and understanding of these compounds is evidently needed at the quasi-2D level, especially considering that magnetic mono- and bilayers of a wide range of 2D quantum magnets have now become accessible.[1−5] Therefore, expanding the knowledge on the magnetic behavior in quasi-2D materials has a great potential in driving the boundaries of materials toward future use in spin electronic-based devices as well as in studying the exceptional quantum properties. The weak interlayer bonding present in van der Waals (vdW) crystals and their extreme sensitivity toward the external perturbation have allowed scientists to explore their interesting physical properties.

In the recent past, external stimuli have been employed to tune the magnetic states in quasi-2D materials via photoexcitation, proton irradiation, strain, gating, doping, pressure, and intercalation.[5−15] Among all, hydrostatic pressure has been used as a disorderless procedure to tune the physical properties of vdW compounds. Pressure on a system of weakly coupled layers affects the bonding and interlayer coupling without destroying the crystal.[2] For instance, a remarkable tuning of the magnetic properties has been seen in $Cr_2Ge_2Te_6$, where ∼9 GPa of pressure significantly increased the Curie temperature (T_C) to a value greater than 250 K, a jump of nearly 184 K from ambient conditions.[16] Previous high-pressure studies (P > 1−47 GPa) conducted on $CrSiTe_3$ reported structural transformations, metallization, spin reorientation transition, and a ferromagnetic to paramagnetic transition with the emergence of superconductivity.[17,18] The most recent work on $CrSiTe_3$ reported a dramatic increase in the T_C by about 100 K with 7.8 GPa of pressure application.[19] The sister compound, $Mn_3Si_2Te_6$ (MST), recently gained a great deal of interest due to the observance of exceptional colossal magneto resistance.[20−22] Recently, MST has shown pressure-dependence of its colossal magneto resistance, along with a semiconductor to metal transition and structural phase transition.[23]

As outlined above, while most of the prior work reported on $Cr_2Si_2Te_6$ (CST) and MST focused on the high-pressure properties, knowledge on their magnetic properties, particularly at lower pressures (<1 GPa), is limited. In this work, we examined the influence of pressure on the magnetic properties

Received: February 16, 2023
Revised: May 7, 2023
Published: May 22, 2023

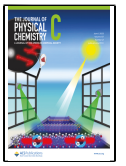

https://doi.org/10.1021/acs.jpcc.3c01091
J. Phys. Chem. C 2023, 127, 10324−10331

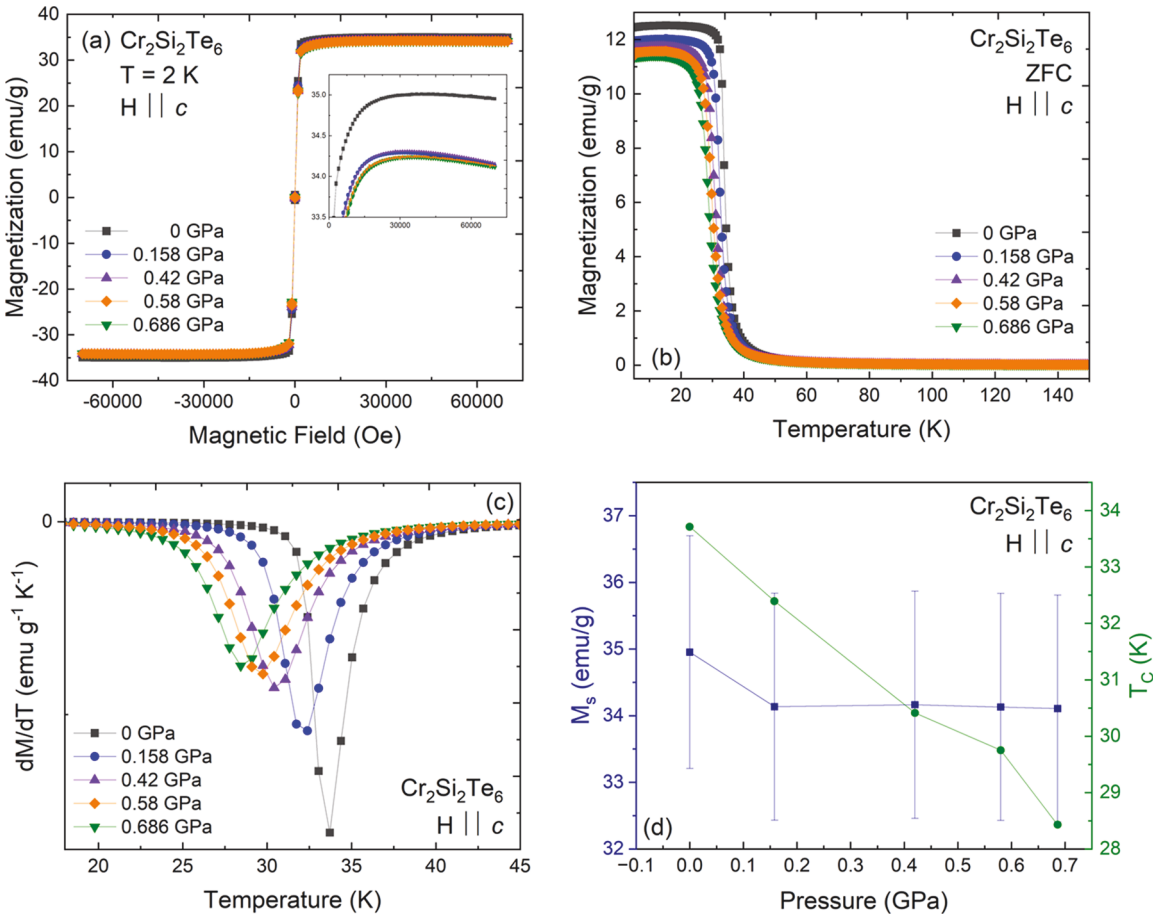

Figure 1. Experimental data collection on $Cr_2Si_2Te_6$ with application of pressure. (a) Isothermal magnetization for the easy axis direction taken at 2 K with ±7 T. Inset: Close-up of the magnetization in the first quadrant. (b) ZFC temperature-dependent magnetization with a 500 Oe magnetic field in the easy axis ($H||c$). (c) Derivative of the magnetization with respect to temperature shown for all applied pressures. (d) Magnetization at 7 T and the ferromagnetic transition temperature plotted as a function of pressure.

of two bulk vdW materials, CST and MST. The application of pressure revealed that the ferromagnetic transition temperature decreases in CST, while the opposite occurs for the ferrimagnet, MST. In MST, the magnetization decreases with the increase in the pressure, and it is not clearly noticed in CST, within the pressure range studied. Density functional theory (DFT) calculations give further insights into the pressure dependence of exchange coupling and magneto-crystalline anisotropy energy in these materials.

The semiconducting material, CST, exhibits a T_C of 32 K with an easy-axis along the *c*-axis.[24] CST crystallizes with a rhombohedral symmetry in a honeycomb network with space group $R\bar{3}$. The Cr ions are arranged in hexagonal planes stacking along the *c*-axis with one-third of layers being composed of Si_2Te_6. Each Cr^{3+} atom ($S = 3/2$) is octahedrally coordinated with Te that are edge-sharing. The insulating compound, MST, is a ferrimagnet whose antiferromagnetic contribution stems from frustration between the three NN interactions between Mn1 (multiplicity of two) and Mn2 sites. MST is often referred to as the sister compound to CST as layers are composed of $MnTe_6$ octahedra sharing an edge with the *ab* plane at the Mn1 site and with Si−Si dimers. However, MST differs in that one-third of the Mn atoms link the layers together by filling the octahedral holes at the Mn2 site.[25] MST has a trigonal crystal structure with space group no. 163[26,27] with T_C reporting between 73 and 78 K.[10,25,28]

METHODS

Experimental Details. Bulk CST and MST crystals were synthesized using a self-flux technique as previously outlined.[28,29] Magnetic measurements were performed using a Quantum Design MPMS 3 with a Superconducting Quantum Interference Device (SQUID) magnetometer. Isothermal magnetization measurements were taken at 2 K with a ±7 T magnetic field. Zero-field cool (ZFC) temperature-dependent magnetization was performed from 2 to 150 K with a measuring field of 500 Oe. Hydrostatic pressure was applied using a BeCu quantum design piston cell. The pressure transmitting medium was Daphne (silicon) oil, and a Pb manometer was used to monitor the pressure in the cell. Compression of the cell length was increasingly applied and only depressurized after the data collection was completed. For CST, we performed pressure measurements with the magnetic field applied parallel to the *c*-axis ($H||c$), out-of-plane measurements. For MST, we fixed the sample along its magnetic easy axis, $H||ab$. See Supporting Information, page S1 and Figure S1, for mounting procedures and pressure determination.

Computational Details. The structural parameters were optimized using the Vienna ab initio simulation package[30,31] within the projector augmented wave method.[32,33] The Perdew−Burke−Ernzerhof generalized gradient approximation[34] was employed to describe exchange correlation effects.

https://doi.org/10.1021/acs.jpcc.3c01091
J. Phys. Chem. C 2023, 127, 10324−10331

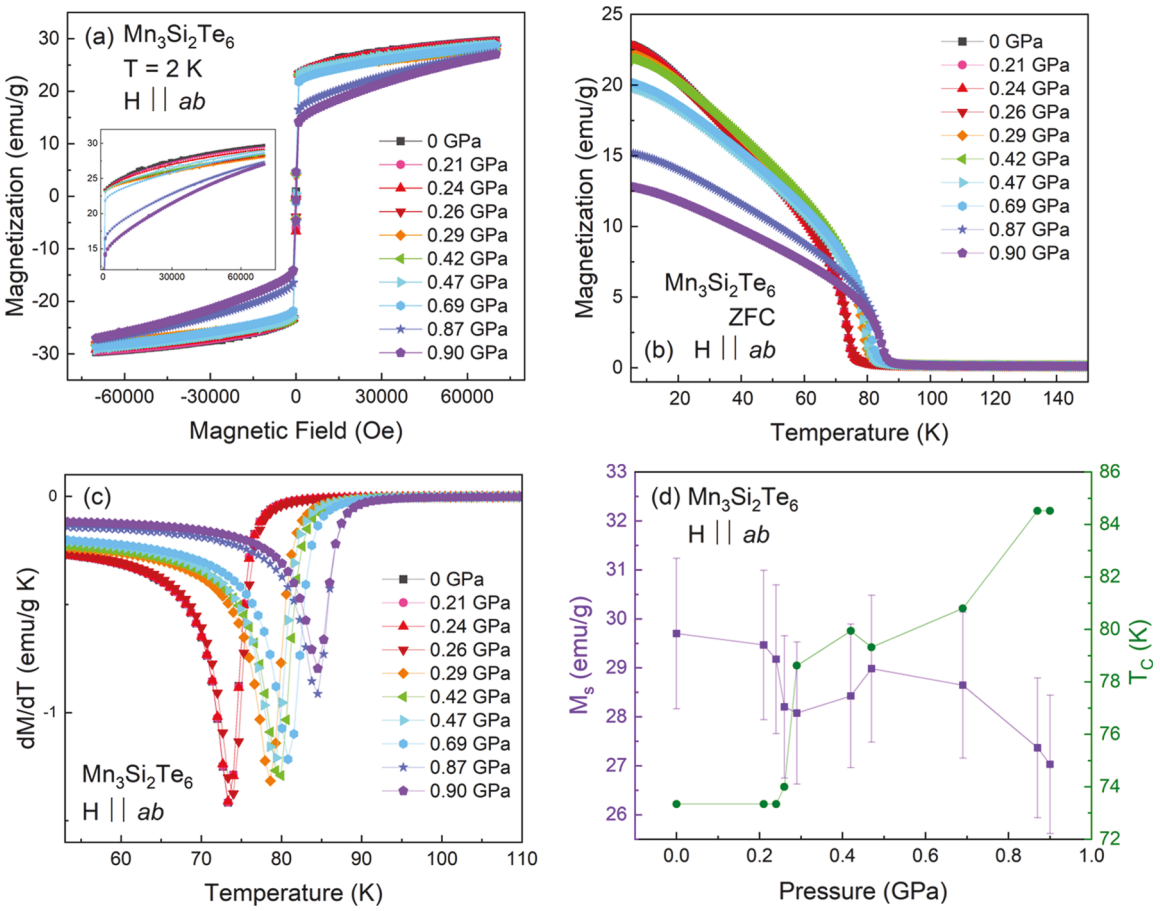

Figure 2. Experimental data collection on $Mn_3Si_2Te_6$ with application of pressure. (a) Isothermal magnetization for the easy axis direction taken at 2 K with ±7 T. Inset: Close-up of the magnetization in the first quadrant. (b) ZFC temperature-dependent magnetization with a 500 Oe magnetic field in the easy axis (H||ab). (c) Derivative of the magnetization with respect to temperature shown for all applied pressures. (d) Magnetization at 7 T and T_C plotted as a function of increasing pressure up to 0.9 GPa.

To better account for the interlayer vdW forces, the optB88-vdW[35,36] form of the non-local vdW functional was used. A cutoff energy of 500 eV was chosen for the plane wave basis set.[37] The structure optimizations were performed until the forces on each atom were less than 5×10^{-3} meV/Å. The hydrostatic pressure effect is included using the PSTRESS tag, which adds stress to the stress tensor and energy generated from the external pressure.

Once the optimized structures were obtained, we used the OpenMX code[38] for calculations of magnetic properties. In these calculations, core electrons are replaced with a norm-conserving pseudopotential[39] with an energy cutoff of 300 Ry. To improve the description for localized d-electrons in Mn and Cr, fully localized limit DFT + U is used.[40,41] The U parameters for CST and MST are taken from the literature.[19,25] The Green function method implemented in OpenMX 3.9[42] is used to calculate exchange coupling constants J_i for up to the 3rd NN. In this approach, the exchange coupling between any pair of magnetic sites can be directly calculated from a single magnetic state. For magneto-crystalline anisotropy energy (MAE), we first performed a full self-consistent calculation without spin−orbit coupling (SOC) to obtain the charge and spin densities. The SOC is subsequently included perturbatively for the configurations with the magnetization aligned in-plane and out-of-plane. The MAE was then determined as the difference in the total band energy between the two.[43]

RESULTS AND DISCUSSION

First, we present and discuss our experimental data gathered on CST, where we applied pressure up to 0.686 GPa. Isothermal magnetization (M−H) measurements were conducted along the easy axis (H||c). Figure 1a plots the M−H data collected at 2 K with ±7 T with various pressures in the range between 0 and 0.686 GPa. A minimal decrease in the saturation magnetization (M_s) at +7 T (maximum limit of our magnetometer) was noted as pressure was increasingly applied. The ZFC temperature variation of magnetization (M−T) collected at various pressures is plotted in Figure 1b with a 500 Oe magnetic field. This plot shows a similar decrease in the magnetization in the ferromagnetic phase (below 34 K). We observed that the M−T curves shifted to the left, indicating a decrease in the magnetic phase transition temperature, T_C, as pressure was increased. Figure 1c displays the derivative of the magnetization with respect to the temperature. It is observed at the maximum applied pressure (0.686 GPa) that T_C decreases to 28 K, in addition to a decrease in the magnitude of the minimum(s) at the largest pressure. This shrinking of the derivative curve, along with the suppression of T_C and magnetization, indicates a decrease in the overall magnetic ordering as similarly seen in the pressure study involving Fe_3GeTe_2.[44] Figure 1d displays the magnetization taken at 7 T and T_C as a function of pressure.

https://doi.org/10.1021/acs.jpcc.3c01091
J. Phys. Chem. C 2023, 127, 10324−10331

Turning our attention to the experiment on MST, we applied hydrostatic pressure up to 0.90 GPa with magnetic field applied along the easy axis (H||ab). Figure 2a displays the isothermal magnetization at 2 K and with ±7 T, collected as a function of applied pressure. At first glance, the M_s at 7 T follows a decreasing trend as pressure is increased to 0.90 GPa. Figure 2b shows the temperature (2−150 K) variation of ZFC magnetization (measuring field: 500 Oe) at various applied pressures (0−0.9 GPa). Interestingly, we noticed an apparent shift of the $M-T$ curves toward the right as the pressure steadily increased. The T_C is estimated in Figure 2c through the magnetization derivative curves, which shows an increase up to 84.52 K at 0.9 GPa, an 11 K jump from the pristine state. The intimate relationship (see Figure 2d) between magnetization and T_C as a function of pressure is not fully understood at this point. Interestingly, this increasing trend in T_C has recently been observed for even higher pressures in MST with results showing a remarkable jump in T_C up to ∼210 K at 8.1 GPa.[23]

To gain additional insight, we also performed first-principles-based calculations for both CST and MST to study the influence of pressure on their magnetic properties. Earlier theoretical calculations have established that the ferromagnetic (FM) phase is the lowest energy spin structure for CST. Our calculations are also carried out on the FM phase. Figure 3 shows a schematic of the dominant in-plane

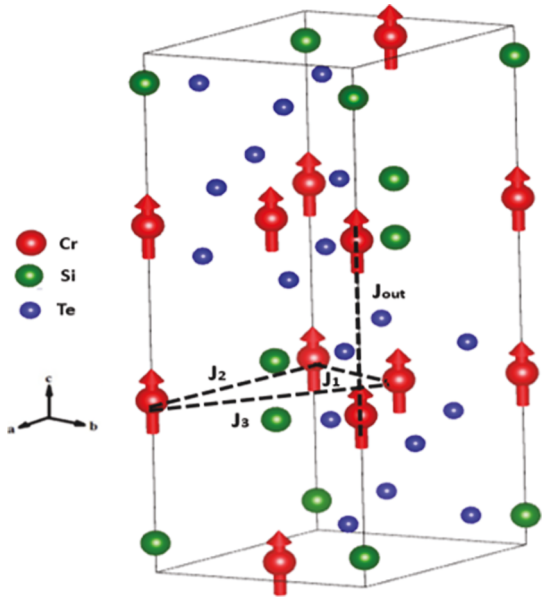

Figure 3. Crystal structure and the spin alignment in $Cr_2Si_2Te_6$. The calculated J parameters between the first, second, and third in-plane nearest Cr neighbors and the interlayer J_{out} are depicted with broken lines.

exchange coupling parameters J_i (i = 1, 2, 3) and out-of-plane parameter J_{out} that are calculated in this work, which are shown as a function of pressure for CST in Figure 4a. As pointed out in the previous work,[19] our calculations confirmed that both the electronic band gap and moments are rather insensitive to U values below 1.0 eV and calculations with U above 1.0 eV produce the incorrect magnetic ground states. Therefore, we performed all calculations both at the GGA and GGA + U levels, using U = 0.5 eV as a comparison to see the impact of U correction.[19,48]

The NN in-plane coupling J_1 is the most dominant interaction followed by J_3. All of the calculated exchange couplings including the interlayer coupling favor ferromagnetic ordering within the entire pressure range considered in this study in accord with the earlier results of Zhang et al.[19] Consistent with the previous findings,[19,45] our data also show a small but positive J_4 which indicates that different layers are only weakly and ferromagnetically coupled. We also observed that while the empirical Hubbard U correction does not change the qualitative behavior in pressure dependence, it greatly enhances the magnitude of the most dominant component J_1. Within this pressure range (0−1 GPa), both intralayer (J_i) and interlayer (J_{out}) couplings exhibit very little dependence on the pressure.

It is known that CST has a weak easy-axis anisotropy,[19] and the strength decreases slowly with pressure in the range 0−8 GPa. Our results also show (Figure 4b) that the system favors the out-of-plane easy-axis and the magnitude of MAE decreases slowly. In CST, T_C is predominately determined by J_i as the MAE shown in Figure 4b is generally too small and unlikely to have a qualitative impact. Since the magnetic moment of the system is dominated by the moments on the transition-metal ions, we present the variation in the total moment of Cr ions per functional unit as a function of pressure in Figure 4c. Within pressure range (0−1 GPa), there is a slight decrease (less than 1%) in the magnetic moment per formula unit. We computed the energy of a low-lying antiferromagnetic (AFM) state where the interlayer spins are oppositely aligned. The total energy differences between the AFM and the FM show a slight increasing trend as a function of pressure as can be seen from Table 1. This result qualitatively indicates that the T_C is likely to show a similar trend as a function of pressure.

Our calculations on the J parameters, magnetic moments, and MAE as a function of pressure indicate that the system is unlikely to show any significant change in T_C within this pressure range (<1 GPa). This result agrees with the earlier reported results below 2 GPa on this compound [19]. In the prior high-pressure (>3 GPa) work [19] reported on much thinner CST flakes, the authors reported a dramatic enhancement (∼100 K) in T_C. Although DFT + U often provides a reasonable estimation for the exchange coupling constants at the equilibrium condition, the pressure-dependent trends presented in Figure 4a,b are insufficient to explain the significant decrease in T_C with pressure. This discrepancy can be partly attributed to the limitation of +U, due to its empirical and overly simplified nature, as it only partially accounts for the strong correlation. Another issue is the determination of U values, as they are generally untransferable[51] and one often varies the parameters to fit the physical observables of interest such as band gap, moment, and so forth.[47] For the analysis of pressure-dependent magnetic properties, the U values once determined are often kept fixed,[49,50] which is often a reasonable assumption, particularly when the pressure is small as in our study. However, in CST, the inclusion of Hubbard U correction has a much more significant impact on J_1 and little effect on the band gap (see Figure S2 in Supporting Information) and the magnetic moments.[19,48] While the issue can potentially be mitigated by performing self-interaction correction,[52−54] GW[55] or dynamical mean-field theory[56] calculations, these methods are computationally too demanding and beyond the scope of this work.

https://doi.org/10.1021/acs.jpcc.3c01091
J. Phys. Chem. C 2023, 127, 10324−10331

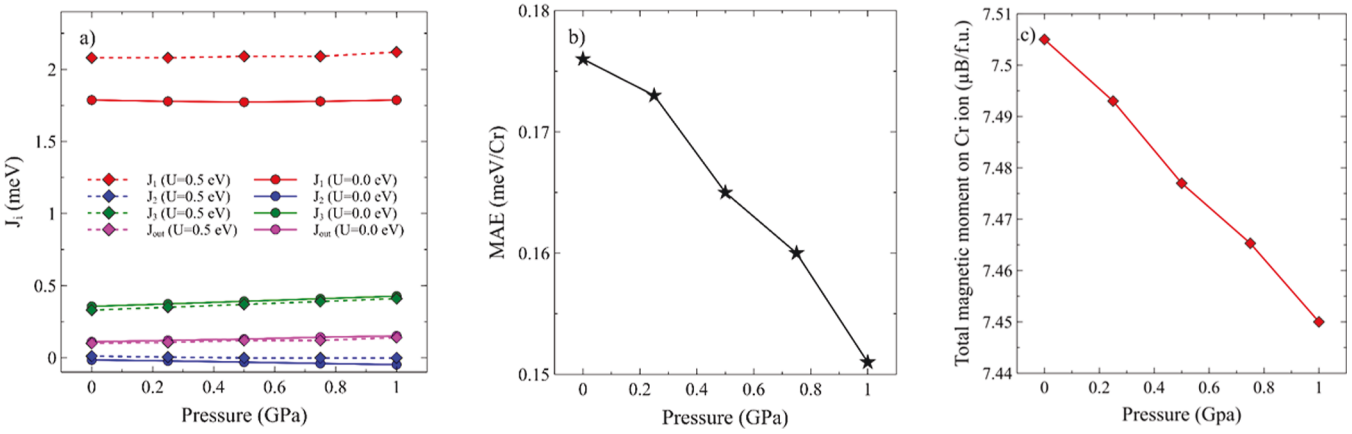

Figure 4. (a) Exchange coupling parameter J_i, (b) MAE, and (c) total magnetic moments on the Cr ions per formula unit as a function of pressure.

Table 1. Total Energy Difference (ΔE) between Interlayer AFM Order and FM Order of CST

U (eV)	P = 0 GPa ΔE (meV)	P = 0.5 GPa ΔE (meV)	P = 1 GPa ΔE (meV)
0.0	37.23	43.66	50.40
0.5	23.88	28.44	33.11

Due to the triangular arrangement in MST as shown in Figure 5, the system is rather frustrated, and several magnetic states are close in energy.[25] To verify that, we consider the total energy differences of several magnetic states: two ferrimagnetic states (FI1 and FI2), two anti-ferromagnetic (AF1 and AF2), and a FM state. The ground state is found to be ferrimagnetic (FI1) with the spins of Mn1 and Mn2 sites oppositely aligned as shown in Figure 5. In the FI2 state, the Mn1 ions have spins antiferromagnetically aligned, while half of the Mn1−Mn2 spins are antiferromagnetically aligned, and the other half are ferromagnetically aligned. Two antiferromagnetic states AF1 and AF2 arise depending on the spin alignment of Mn2. In AF1, the Mn2 spin is aligned similarly to the nearest Mn1, while in AF2, the Mn2 spins are oppositely aligned to the nearest Mn1.[25]

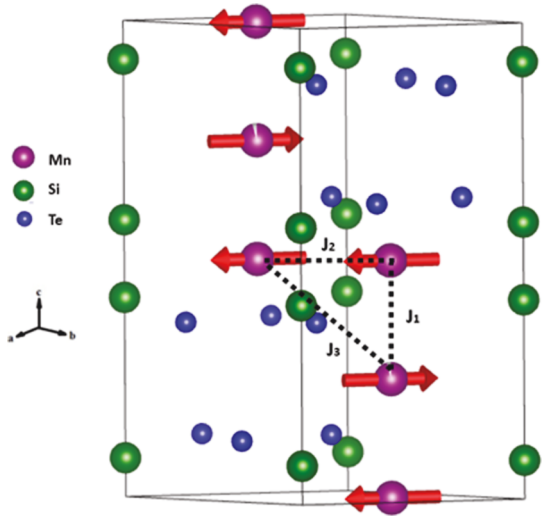

Figure 5. Crystal structure of $Mn_3Si_2Te_6$. FI1 is the ground state whose magnetic configuration examined by first-principles calculation is shown.

Previous reports suggest that GGA performs well for MST in predicting both the Curie temperature and the Curie−Weiss temperature based on the calculated exchange parameters.[23,25] Therefore, we will primarily focus our discussion on the GGA results, with the results for GGA + U provided as a reference. Table 2 shows the calculated relative energies of the magnetic states calculated with GGA and GGA + U compared to those of the ferrimagnetic ground state (FI1), which agrees with the previous findings obtained using the linearized augmented plane-wave code.[25] These calculations also confirm that FI1 is the ground state. Further calculations with hydrostatic pressure were done on the FI1 state only. The three dominant exchange coupling parameters are depicted in Figure 5. Here J_1, J_2, and J_3 are the couplings between NNs Mn1−Mn2, Mn1−Mn1, and second NNs Mn1−Mn2.

Figure 6a shows the pressure dependence of exchange coupling constants calculated for both U = 0 and U = 3.0 eV. Intial observation of the overall qualitative pressure dependence shows that the trend remains similar for each exchange coupling constant as pressure increases. However, it is clear that the use of U correction reduces the strengths of the exchange couplings in MST. The application of pressure affects mostly the J_1 parameter, which is the dominant interaction that favors the moments of the corresponding Mn1−Mn2 pairs to be antiferromagnetically ordered. As the pressure increases, the orbitals become more delocalized. Ferromagnetic ordering is favored when the orbitals share the same space and are orthogonal. Covalent interaction favors antiferromagnetic ordering which is the case in this system. On the other hand, J_2 and J_3 are similar in strength at the GGA level, and both favor antiferromagnetic ordering of the respective pairs leading to a frustrated system. The increase of J_1 with pressure indicates the tendency to stabilize the FI1 state. In Figure 6b, we show the magnetic anisotropy energy as a function of the applied pressure. Our calculations predict an easy-plane anisotropy with MAE of about 0.68 meV/Mn at zero pressure which is in close agreement with the previous work,[25] and the magnitude decreases monotonically by about 15% at P = 1.0 GPa. In Figure 6c, we show the total magnetic moments on the Mn atoms per formula unit as a function of applied pressure. Our calculations revealed a decreasing trend as seen in the experiment within the pressure range 0−1 GPa.

To qualitatively understand the trend of Curie temperature evolution with pressure, we employ a simple and widely used method based on mean-field approximation,[46] where the Curie

https://doi.org/10.1021/acs.jpcc.3c01091
J. Phys. Chem. C 2023, 127, 10324−10331

Table 2. Relative Energies of Different Magnetic Phases of MST in meV/Mn

	ΔE (meV/Mn) U = 0.0 eV					
pressure (GPa)	0	0.25	0.5	0.75	1	reported[25] (0 GPa)
FI1 (GS)	0	0	0	0	0	0
AF1	23.36	25.36	27.44	30.11	32.92	19.1
AF2	33.29	34.02	35.1	35.96	37.19	31.5
FI2	32.97	34.57	36.37	38.37	40.59	32.2
FM	102.98	104.3	105.9	107.1	108.6	105.4
	ΔE (meV/Mn) U = 3.0 eV					
FI1 (GS)	0	0	0	0	0	
AF1	15.96	17.37	18.77	20.63	22.49	
AF2	13.61	14.42	15.32	16.10	17.19	
FI2	16.28	17.41	18.64	20.0	21.54	
FM	43.98	46.62	49.48	52.74	56.42	43

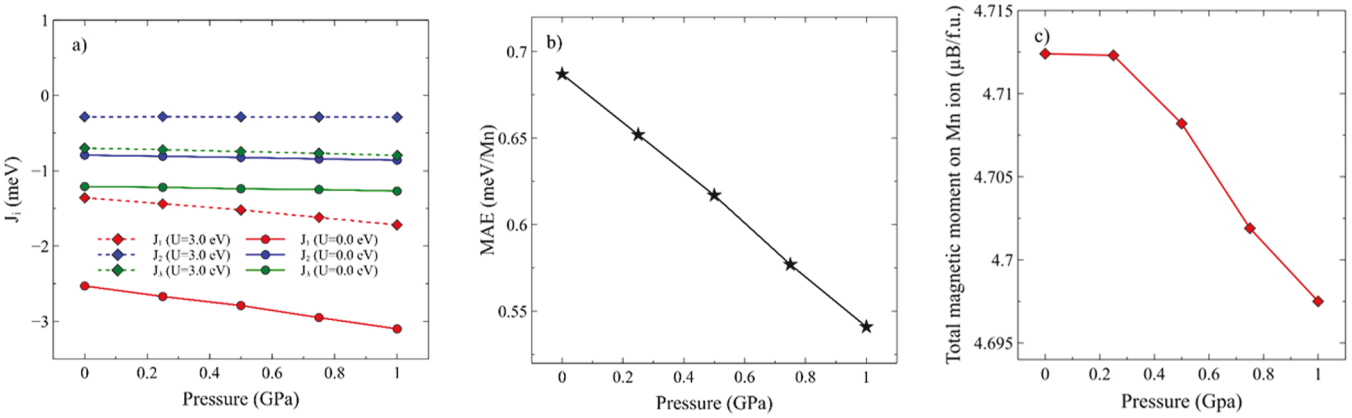

Figure 6. Pressure dependence of the (a) exchange coupling parameters for MST, (b) MAE, and (c) total magnetic moments on the Mn_3 ions per formula unit.

temperature is estimated from the total energy difference between the ground state and the competing excited state.[23,25] As shown in Table 2, the relative ordering between the AF1 and AF2 changes with GGA + U compared to GGA. Relative energies of both the AF1 and AF2 increases compared to the ground state, which indicates that the T_C will also increase with pressure in accord with the experimental results. The stabilization of the ground state as indicated by the increase in J_1 also indicates that the energy difference between the ground and the paramagnetic state is likely to increase leading to a rise in T_C.

CONCLUSIONS

In this work, we investigated the pressure-dependent magnetic properties of two quasi-2D magnets, $Cr_2Si_2Te_6$ and $Mn_3Si_2Te_6$, by employing the Quantum Design Magnetometer coupled with theoretical calculations. In the case of CST, we find that the Curie temperature is decreased from 34 to 28 K as the pressure is increased from 0 to 0.686 GPa, though the saturation magnetization is marginally decreased within the pressure range applied. Moreover, it will be important to observe the coercivity and the interplanar distance to corroborate the results from previous high-pressure studies. It also seems that the literature will benefit from a comprehensive magnetization study in the high-pressure regime to bring together the results of pressure-enhanced ferromagnetism in ref 19 up to 7.8 GPa and a structural transition causing a ferromagnetic to paramagnetic transition leading to superconductivity at 7.5 GPa,[18] to a spin reorientation at ∼ 6 GPa inducing metallization.[17] Quite intriguingly, in the case of MST, the T_C is found to increase by 11 K upon increase of pressure from 0 to 0.9 GPa. Recent rich phenomena has been demonstrated in high pressure studies on MST such as pressure-induced semiconductor to metal transition between 1.5 and 2.5 GPa and using pressure to control the apparent colossal magnetoresistance in this material.[20,23] First-principles calculations on these materials are carried out to understand the effects of pressure on the magnetic properties such as exchange coupling parameters and magnetic anisotropy energies. In CST, the exchange coupling parameters exhibit very little dependence on the pressure within the range 0−1 GPa in accord with earlier theoretical calculations.[19] We find that the exchange coupling in MST is strongly frustrated, and the first NN interaction is the most dominant component that shows a dependence on pressure. DFT calculations at the GGA + U level indicate that the nearest neighbor exchange couplings and MAE change monotonically with pressure up to 1 GPa. A qualitative estimate of the change in T_C with pressure shows that T_C is likely to increase with pressure in accord with experimental results. To gain deeper insights and further expand this work, we are currently performing synchrotron-based high-pressure X-ray magnetic circular dichroism measurements and pressure-dependent Raman measurements.

https://doi.org/10.1021/acs.jpcc.3c01091
J. Phys. Chem. C 2023, 127, 10324−10331

■ ASSOCIATED CONTENT

Supporting Information

The Supporting Information is available free of charge at https://pubs.acs.org/doi/10.1021/acs.jpcc.3c01091.

Description of high-pressure cell sample mounting and calculation of the band structure (PDF)

■ AUTHOR INFORMATION

Corresponding Authors

Srinivasa R. Singamaneni − *Department of Physics, The University of Texas at El Paso, El Paso, Texas 79968, United States*; Email: srao@utep.edu

Po-Hao Chang − *Department of Physics, The University of Texas at El Paso, El Paso, Texas 79968, United States*; Email: changpohao@gmail.com

Authors

Rubyann Olmos − *Department of Physics, The University of Texas at El Paso, El Paso, Texas 79968, United States;* Present Address: Department of Physics and Astronomy, Rice University, Houston, TX 77005, United States; orcid.org/0000-0001-8190-6637

Prakash Mishra − *Computational Science Program, The University of Texas at El Paso, El Paso, Texas 79968, United States;* orcid.org/0000-0002-7304-777X

Rajendra R. Zope − *Department of Physics, The University of Texas at El Paso, El Paso, Texas 79968, United States*

Tunna Baruah − *Department of Physics, The University of Texas at El Paso, El Paso, Texas 79968, United States*

Yu Liu − *Condensed Matter Physics and Materials Science Department, Brookhaven National Laboratory, Upton, New York 11973, United States;* Present Address: Los Alamos National Laboratory, Los Alamos, NM 87545, United States.; orcid.org/0000-0001-8886-2876

Cedomir Petrovic − *Condensed Matter Physics and Materials Science Department, Brookhaven National Laboratory, Upton, New York 11973, United States;* orcid.org/0000-0001-6063-1881

Complete contact information is available at: https://pubs.acs.org/10.1021/acs.jpcc.3c01091

Notes

The authors declare no competing financial interest.

■ ACKNOWLEDGMENTS

This material is based upon work supported by the National Science Foundation Graduate Research Fellowship Program under grant no. 1842494. Any opinions, findings, and conclusions or recommendations expressed in this material are those of the author(s) and do not necessarily reflect the views of the National Science Foundation. S.R.S., R.O., P.M., and T.B. acknowledge support from the NSF-DMR (Award no. 2105109). S.R.S. acknowledges support from NSF-MRI (Award no. 2018067). PH.C., T.B., and R.R.Z. acknowledge support from the US Department of Energy, Office of Science, Office of Basic Energy Sciences, as part of the Computational Chemical Sciences Program under Award no. DE-SC0018331. Support for computational time at the Texas Advanced Computing Center directly and through NSF Grant no. TG-DMR090071 and NERSC is gratefully acknowledged. Work at Brookhaven National Laboratory was supported by the U.S. DOE under Contract no. DESC0012704 (materials synthesis).

■ REFERENCES

(1) Duong, D. L.; Yun, S. J.; Lee, Y. H. Van der Waals Layered Materials: Opportunities and Challenges. *ACS Nano* **2017**, *11*, 11803−11830.

(2) Ajayan, P.; Kim, P.; Banerjee, K. Two-Dimensional Van der Waals Materials. *Phys. Today* **2016**, *69*, 38−44.

(3) Gong, C.; Zhang, X. Two-Dimensional Magnetic Crystals and Emergent Heterostructure Devices. *Science* **2019**, *363*, No. eaav4450.

(4) Huang, B.; Clark, G.; Navarro-Moratalla, E.; Klein, D. R.; Cheng, R.; Seyler, K. L.; Zhong, D.; Schmidgall, E.; McGuire, M. A.; Cobden, D. H.; Yao, W.; Xiao, D.; Jarillo-Herrero, P.; Xu, X. Layer-Dependent Ferromagnetism in a van der Waals Crystal Down to the Monolayer Limit. *Nature* **2017**, *546*, 270−273.

(5) Wang, Q. H.; Bedoya-Pinto, A.; Blei, M.; Dismukes, A. H.; Hamo, A.; Jenkins, S.; Koperski, M.; Liu, Y.; Sun, Q.-C.; Telford, E. J.; Kim, H. H.; Augustin, M.; Vool, U.; Yin, J.-X.; Li, L. H.; Falin, A.; Dean, C. R.; Casanova, F.; Evans, R. F. L.; Chshiev, M.; Mishchenko, A.; Petrovic, C.; He, R.; Zhao, L.; Tsen, A. W.; Gerardot, B. D.; Brotons-Gisbert, M.; Guguchia, Z.; Roy, X.; Tongay, S.; Wang, Z.; Hasan, M. Z.; Wrachtrup, J.; Yacoby, A.; Fert, A.; Parkin, S.; Novoselov, K. S.; Dai, P.; Balicas, L.; Santos, E. J. G. The Magnetic Genome of Two-Dimensional van der Waals Materials. *ACS Nano* **2022**, *16*, 6960−7079.

(6) Padmanabhan, P.; Buessen, F. L.; Tutchton, R.; Kwock, K. W. C.; Gilinsky, S.; Lee, M. C.; McGuire, M. A.; Singamaneni, S. R.; Yarotski, D. A.; Paramekanti, A.; Zhu, J.-X.; Prasankumar, R. P. Coherent Helicity-Dependent Spin-Phonon Oscillations in the Ferromagnetic van der Waals Crystal CrI_3. *Nat. Commun.* **2022**, *13*, 4473.

(7) Singamaneni, S. R.; Martinez, L. M.; Niklas, J.; Poluektov, O. G.; Yadav, R.; Pizzochero, M.; Yazyev, O. V.; McGuire, M. A. Light Induced Electron Spin Resonance Properties of van der Waals CrX_3 (X = Cl, I) Crystals. *Appl. Phys. Lett.* **2020**, *117*, 082406.

(8) Olmos, R.; Alam, S.; Chang, P.-H.; Gandha, K.; Nlebedim, I. C.; Cole, A.; Tafti, F.; Zope, R. R.; Singamaneni, S. R. Pressure Dependent Magnetic Properties on Bulk $CrBr_3$ Single Crystals. *J. Alloys Compd.* **2022**, *911*, 165034.

(9) Martinez, L. M.; Iturriaga, H.; Olmos, R.; Shao, L.; Liu, Y.; Mai, T. T.; Petrovic, C.; Hight Walker, A. R.; Singamaneni, S. R. Enhanced Magnetization in Proton Irradiated $Mn_3Si_2Te_6$ van der Waals Crystals. *Appl. Phys. Lett.* **2020**, *116*, 172404.

(10) Olmos, R.; Delgado, J.; Iturriaga, H.; Martinez, L. M.; Saiz, C. L.; Shao, L.; Liu, Y.; Petrovic, C.; Singamaneni, S. R. Critical Phenomena of the Layered Ferrimagnet $Mn_3Si_2Te_6$ Following Proton Irradiation. *J. Appl. Phys.* **2021**, *130*, 013902.

(11) Mak, K. F.; Shan, J.; Ralph, D. C. Probing and Controlling Magnetic States in 2D Layered Magnetic Materials. *Nat. Rev. Phys.* **2019**, *1*, 646−661.

(12) Jiang, S.; Li, L.; Wang, Z.; Mak, K. F.; Shan, J. Controlling Magnetism in 2D CrI_3 by Electrostatic Doping. *Nat. Nanotechnol.* **2018**, *13*, 549−553.

(13) Wang, Z.; Zhang, T.; Ding, M.; Dong, B.; Li, Y.; Chen, M.; Li, X.; Huang, J.; Wang, H.; Zhao, X.; Li, Y.; Li, D.; Jia, C.; Sun, L.; Guo, H.; Ye, Y.; Sun, D.; Chen, Y.; Yang, T.; Zhang, J.; Ono, S.; Han, Z.; et al. Electric-Field Control of Magnetism in a Few-Layered van der Waals Ferromagnetic Semiconductor. *Nat. Nanotechnol.* **2018**, *13*, 554−559.

(14) Wang, N.; Tang, H.; Shi, M.; Zhang, H.; Zhuo, W.; Liu, D.; Meng, F.; Ma, L.; Ying, J.; Zou, L.; Sun, Z.; Chen, X. Transition from Ferromagnetic Semiconductor to Ferromagnetic Metal with Enhanced Curie Temperature in $Cr_2Ge_2Te_6$ via Organic Ion Intercalation. *J. Am. Chem. Soc.* **2019**, *141*, 17166−17173.

(15) Liu, Y.; Susilo, R. A.; Lee, Y.; Abeykoon, A. M. M.; Tong, X.; Hu, Z.; Stavitski, E.; Attenkofer, K.; Ke, L.; Chen, B.; Petrovic, C. Short-Range Crystalline Order-Tuned Conductivity in $Cr_2Si_2Te_6$ van der Waals Magnetic Crystals. *ACS Nano* **2022**, *16*, 13134−13143.

(16) Bhoi, D.; Gouchi, J.; Hiraoka, N.; Zhang, Y.; Ogita, N.; Hasegawa, T.; Kitagawa, K.; Takagi, H.; Kim, K. H.; Uwatoko, Y. Nearly Room-Temperature Ferromagnetism in a Pressure-Induced

Correlated Metallic State of the van der Waals Insulator $CrGeTe_3$. *Phys. Rev. Lett.* **2021**, *127*, 217203.
(17) Xu, K.; Yu, Z.; Xia, W.; Xu, M.; Mai, X.; Wang, L.; Guo, Y.; Miao, X.; Xu, M. Unique 2D−3D Structure Transformations in Trichalcogenide $CrSiTe_3$ under High Pressure. *J. Phys. Chem. C* **2020**, *124*, 15600−15606.
(18) Cai, W.; Sun, H.; Xia, W.; Wu, C.; Liu, Y.; Liu, H.; Gong, Y.; Yao, D.-X.; Guo, Y.; Wang, M. Pressure-Induced Superconductivity and Structural Transition in Ferromagnetic $CrSiTe_3$. *Phys. Rev. B* **2020**, *102*, 144525.
(19) Zhang, C.; Gu, Y.; Wang, L.; Huang, L.-L.; Fu, Y.; Liu, C.; Wang, S.; Su, H.; Mei, J.-W.; Zou, X.; Dai, J.-F. Pressure-Enhanced Ferromagnetism in Layered $CrSiTe_3$ Flakes. *Nano Lett.* **2021**, *21*, 7946−7952.
(20) Ni, Y.; Zhao, H.; Zhang, Y.; Hu, B.; Kimchi, I.; Cao, G. Colossal Magnetoresistance via Avoiding Fully Polarized Magnetization in the Ferrimagnetic Insulator $Mn_3Si_2Te_6$. *Phys. Rev. B* **2021**, *103*, L161105.
(21) Zhang, Y.; Ni, Y.; Zhao, H.; Hakani, S.; Ye, F.; DeLong, L.; Kimchi, I.; Cao, G. Control of Chiral Orbital Currents in a Colossal Magnetoresistance Material. *Nature* **2022**, *611*, 467−472.
(22) Liu, Y.; Hu, Z.; Abeykoon, M.; Stavitski, E.; Attenkofer, K.; Bauer, E. D.; Petrovic, C. Polaronic Transport and Thermoelectricity in $Mn_3Si_2Te_6$ Single Crystals. *Phys. Rev. B* **2021**, *103*, 245122.
(23) Wang, J.; Wang, S.; He, X.; Zhou, Y.; An, C.; Zhang, M.; Zhou, Y.; Han, Y.; Chen, X.; Zhou, J.; Yang, Z. Pressure Engineering of Colossal Magnetoresistance in the Ferrimagnetic Nodal-Line Semiconductor $Mn_3Si_2Te_6$. *Phys. Rev. B* **2022**, *106*, 045106.
(24) Casto, L. D.; Clune, A. J.; Yokosuk, M. O.; Musfeldt, J. L.; Williams, T. J.; Zhuang, H. L.; Lin, M.-W.; Xiao, K.; Hennig, R. G.; Sales, B. C.; Yan, J.-Q.; Mandrus, D. Strong Spin-Lattice Coupling in $CrSiTe_3$. *APL Mater.* **2015**, *3*, 041515.
(25) May, A. F.; Liu, Y.; Calder, S.; Parker, D. S.; Pandey, T.; Cakmak, E.; Cao, H.; Yan, J.; McGuire, M. A. Magnetic Order and Interactions in Ferrimagnetic $Mn_3Si_2Te_6$. *Phys. Rev. B* **2017**, *95*, 174440.
(26) Rimet, R.; Schlenker, C.; Vincent, H. A New Semiconducting Ferrimagnet: A Silicon Manganese Telluride. *J. Magn. Magn. Mater.* **1981**, *25*, 7−10.
(27) Vincent, H.; Leroux, D.; Bijaoui, D.; Rimet, R.; Schlenker, C. Crystal Structure of $Mn_3Si_2Te_6$. *J. Solid State Chem.* **1986**, *63*, 349−352.
(28) Liu, Y.; Petrovic, C. Critical Behavior and Magnetocaloric Effect in $Mn_3Si_2Te_6$. *Phys. Rev. B* **2018**, *98*, 064423.
(29) Liu, Y.; Petrovic, C. Anisotropic Magnetic Entropy Change in $Cr_2X_2Te_6$ (X = Si and Ge). *Phys. Rev. Mater.* **2019**, *3*, 014001.
(30) Kresse, G.; Furthmüller, J. Efficiency of ab-initio Total Energy Calculations for Metals and Semiconductors Using a Plane-Wave Basis Set. *Comput. Mater. Sci.* **1996**, *6*, 15−50.
(31) Kresse, G.; Furthmüller, J. Efficient Iterative Schemes for ab initio Total-Energy Calculations Using a Plane-Wave Basis Set. *Phys. Rev. B: Condens. Matter Mater. Phys.* **1996**, *54*, 11169−11186.
(32) Blöchl, P. E. Projector Augmented-Wave Method. *Phys. Rev. B: Condens. Matter Mater. Phys.* **1994**, *50*, 17953−17979.
(33) Kresse, G.; Joubert, D. From Ultrasoft Pseudopotentials to the Projector Augmented-Wave Method. *Phys. Rev. B: Condens. Matter Mater. Phys.* **1999**, *59*, 1758−1775.
(34) Perdew, J. P.; Burke, K.; Ernzerhof, M. Generalized Gradient Approximation Made Simple. *Phys. Rev. Lett.* **1996**, *77*, 3865−3868.
(35) Klimeš, J.; Bowler, D. R.; Michaelides, A. Chemical Accuracy for the van der Waals Density Functional. *J. Phys.: Condens. Matter* **2010**, *22*, 022201.
(36) Klimeš, J.; Bowler, D. R.; Michaelides, A. Van der Waals Density Functionals Applied to Solids. *Phys. Rev. B: Condens. Matter Mater. Phys.* **2011**, *83*, 195131.
(37) Monkhorst, H. J.; Pack, J. D. Special Points for Brillouin-Zone Integrations. *Phys. Rev. B: Condens. Matter Mater. Phys.* **1976**, *13*, 5188−5192.
(38) Ozaki, T. Variationally Optimized Atomic Orbitals for Large-Scale Electronic Structures. *Phys. Rev. B: Condens. Matter Mater. Phys.* **2003**, *67*, 155108.
(39) Vanderbilt, D. Soft Self-Consistent Pseudopotentials in a Generalized Eigenvalue Formalism. *Phys. Rev. B: Condens. Matter Mater. Phys.* **1990**, *41*, 7892−7895.
(40) Anisimov, V. I.; Solovyev, I. V.; Korotin, M. A.; Czyżyk, M. T.; Sawatzky, G. A. Density-Functional Theory and NiO Photoemission Spectra. *Phys. Rev. B: Condens. Matter Mater. Phys.* **1993**, *48*, 16929−16934.
(41) Ryee, S.; Han, M. J. The Effect of Double Counting, Spin Density, and Hund Interaction in the Different DFT+U Functionals. *Sci. Rep.* **2018**, *8*, 9559.
(42) Terasawa, A.; Matsumoto, M.; Ozaki, T.; Gohda, Y. Efficient Algorithm Based on Liechtenstein Method for Computing Exchange Coupling Constants Using Localized Basis Set. *J. Phys. Soc. Jpn.* **2019**, *88*, 114706.
(43) Chang, P.-H.; Fang, W.; Ozaki, T.; Belashchenko, K. D. Voltage-Controlled Magnetic Anisotropy in Antiferromagnetic MgO-Capped MnPt Films. *Phys. Rev. Mater.* **2021**, *5*, 054406.
(44) Ding, S.; Liang, Z.; Yang, J.; Yun, C.; Zhang, P.; Li, Z.; Xue, M.; Liu, Z.; Tian, G.; Liu, F.; Wang, W.; Yang, W.; Yang, J. Ferromagnetism in two-dimensional Fe_3GeTe_2; Tunability by hydrostatic pressure. *Phys. Rev. B* **2021**, *103*, 094429.
(45) Zhang, J.; Cai, X.; Xia, W.; Liang, A.; Huang, J.; Wang, C.; Yang, L.; Yuan, H.; Chen, Y.; Zhang, S.; Guo, Y.; Liu, Z.; Li, G. Unveiling Electronic Correlation and the Ferromagnetic Superexchange Mechanism in the van der Waals Crystal $CrSiTe_3$. *Phys. Rev. Lett.* **2019**, *123*, 047203.
(46) Shahjahan, M.; Toyoda, M.; Oguchi, T. Ferromagnetic Half Metallicity in Doped Chalcopyrite Semiconductors $Cu(Al_{1-x}A_x)Se_2$ (A = 3 d Transition-Metal Atoms). *J. Phys. Soc. Jpn.* **2014**, *83*, 094702.
(47) Kang, S.; Kang, S.; Kim, H. S.; Yu, J. Field-Controlled Quantum Anomalous Hall Effect in Electron-Doped $CrSiTe_3$ Monolayer. *npj 2D Mater. Appl.* **2023**, *7*, 13.
(48) Kang, S.; Kang, S.; Yu, J. Effect of Coulomb Interactions on the Electronic and Magnetic Properties of Two-Dimensional $CrSiTe_3$ and $CrGeTe_3$ Materials. *J. Electron. Mater.* **2019**, *48*, 1441−1445.
(49) Shen, Z. X.; Bo, X.; Cao, K.; Wan, X.; He, L. Magnetic Ground State and Electron-Doping Tuning of Curie Temperature in Fe_3GeTe_2: First-Principles Studies. *Phys. Rev. B* **2021**, *103*, 085102.
(50) Ahmad, A. S.; Liang, Y.; Dong, M.; Zhou, X.; Fang, L.; Xia, Y.; Dai, J.; Yan, X.; Yu, X.; Dai, J.; et al. Pressure-Driven Switching of Magnetism in Layered $CrCl_3$. *Nanoscale* **2020**, *12*, 22935−22944.
(51) Tolba, S. A.; Gameel, K. M.; Ali, B. A.; Almossalami, H. A.; Allam, N. K. The DFT+ U: Approaches, Accuracy, and Applications. *Density Functional Calculations-Recent Progresses of Theory and Application*; IntechOpen, 2018; Vol. *1*, p 5772.
(52) Perdew, J. P.; Zunger, A. Self-Interaction Correction to Density-Functional Approximations for Many-Electron Systems. *Phys. Rev. B: Condens. Matter Mater. Phys.* **1981**, *23*, 5048−5079.
(53) Zope, R. R.; Yamamoto, Y.; Diaz, C. M.; Baruah, T.; Peralta, J. E.; Jackson, K. A.; Santra, B.; Perdew, J. P. A Step in the Direction of Resolving the Paradox of Perdew-Zunger Self-Interaction Correction. *J. Chem. Phys.* **2019**, *151*, 214108.
(54) Yamamoto, Y.; Baruah, T.; Chang, P. H.; Romero, S.; Zope, R. R. Self-Consistent Implementation of Locally Scaled Self-Interaction-Correction Method. *J. Chem. Phys.* **2023**, *158*, 064114.
(55) Aryasetiawan, F.; Gunnarsson, O. The **GW** method. *Rep. Prog. Phys.* **1998**, *61*, 237−312.
(56) Aoki, H.; Tsuji, N.; Eckstein, M.; Kollar, M.; Oka, T.; Werner, P. Nonequilibrium Dynamical Mean-Field Theory and its Applications. *Rev. Mod. Phys.* **2014**, *86*, 779−837.

https://doi.org/10.1021/acs.jpcc.3c01091
J. Phys. Chem. C 2023, 127, 10324−10331